ChemComm

COMMUNICATION

View Article Online
View Journal | View Issue



Cite this: *Chem. Commun.*, 2023, 59, 7639

Received 8th December 2022,
Accepted 22nd May 2023

DOI: 10.1039/d2cc06687d

rsc.li/chemcomm



# Bifunctional chimera for ligand-directed photo-degradation of oncogenic microRNA†

Chen Li, Jin Wang, Yan Wang, Yi Feng, Jinbo Li * and Yan Zhang *

**Targeted inhibition of oncogenic microRNAs provides a promising anti-cancer approach. Here, we report a bifunctional chimera for ligand-directed regulation of target oncogenic precursor microRNA through photo-degradation. Chimeric TGP-210-Ppa with photosensitizer pyropheophorbide a (Ppa) linked with the ligand of the oncogenic precursor miR-210 was able to bind specifically to oncogenic pre-miRNA and produce $^1O_2$ under red light irradiation to degrade the target pre-miRNA. This bifunctional chimera-based modification of precursor microRNA serves as a unique method for target gene regulation since photo-irradiation was able to provide temporal–spatial resolution. We demonstrated that TGP-210-Ppa prevented the generation of functional miR-210 in breast cancer cells in a photocontrollable manner. This also successfully reversed the downstream oncogenic signaling pathway mediated by miR-210 to promote cancer cell death.**

As a class of endogenous gene regulators, microRNAs (miRNAs) have been found to extensively participate in cancer progression.[1] Suppression of oncogenic miRNAs thus represents a promising anti-cancer strategy.[2,3] In addition to antisense oligonucleotides capable of blocking miRNA function through Watson–Crick base pairing-based hybridization,[4] small molecules that directly bind to the secondary structures of miRNAs are emerging as a novel type of miRNA inhibitor.[5] For example, xanthone derivatives,[6] aminoglycosides,[7,8] and ether-amide derivatives[9] have been reported to selectively bind and inhibit target miRNAs in living cells. To further enhance the potency of small-molecule inhibitors, the Disney group developed bifunctional chimeras containing small-molecule ligands of precursor miRNAs for targeted miRNA degradation.[10,11] Ribonuclease-targeting chimera (RIBOTAC) comprising a small-molecule miRNA ligand linked with an RNase recruiter is validated to induce miRNA degradation by bringing RNase in close proximity to the target miRNA.[12,13] This approach has been demonstrated to degrade oncogenic miRNAs such as miR-96,[14] miR-210,[15] miR-17-92,[16] and miR-21.[12] These achievements highlight the promise of small-molecule chimeras for miRNA inhibition.

Singlet oxygen ($^1O_2$) is a reactive oxygen species (ROS) that is highly detrimental toward biomolecules, including nucleic acids, proteins and lipids.[17,18] Exposure to $^1O_2$ is known to cause oxidative damage to adjacent biomolecules and lead to malfunction of the oxidized biomolecules.[19,20] Photosensitizers with strong absorption at long wavelengths have been widely adopted for biomedical applications to generate $^1O_2$ in spatio-temporal- and dose-controllable manners.[21,22] The integration of photosensitizers with photoirradiation to produce excessive $^1O_2$ has led to the discovery of photodynamic therapy (PDT) as a powerful anti-cancer modality.[23,24] A more deliberate approach, named chromophore-assisted light inactivation (CALI), has been developed to selectively inactivate proteins in living cells by pre-installation of photosensitizers onto the target followed by meticulous light illumination to generate $^1O_2$.[25,26] However, the possibility of using $^1O_2$ to precisely inactivate miRNAs in living cells has been little reported.

Here we report a novel small-molecule chimera, **TGP-210-Ppa**, for targeted inhibition of miR-210 in living cancer cells (Scheme 1). **TGP-210-Ppa** consists of the small-molecule ligand, **TGP-210**, against precursor miR-210 (pre-miR-210) and the organic photosensitizer, pyropheophorbide a (Ppa). Upon ligand-directed binding of **TGP-210-Ppa** to pre-miR-210, red light irradiation is implemented to excite Ppa to produce $^1O_2$ to oxidize riboguanosine (rG) into 8-oxo-rG, causing the mutation and dysfunction of pre-miR-210.

The chemical structure of **TGP-210-Ppa** is shown in Fig. 1a. The two functional units, **TGP-210** and Ppa were readily conjugated together using an amide condensation strategy with ethylenediamine as the linker (Fig. S1, ESI†). The structure of the purified **TGP-210-Ppa** was confirmed by electrospray ionization-mass spectrometry (ESI-MS) (Fig. S2, ESI†). The

*State Key Laboratory of Analytical Chemistry for Life Sciences, Jiangsu Key Laboratory of Advanced Organic Materials, School of Chemistry and Chemical Engineering, Chemistry and Biomedicine Innovation Center, Nanjing University, Nanjing 210023, China. E-mail: jinboli@nju.edu.cn, njuzy@nju.edu.cn*

† Electronic supplementary information (ESI) available. See DOI: https://doi.org/10.1039/d2cc06687d

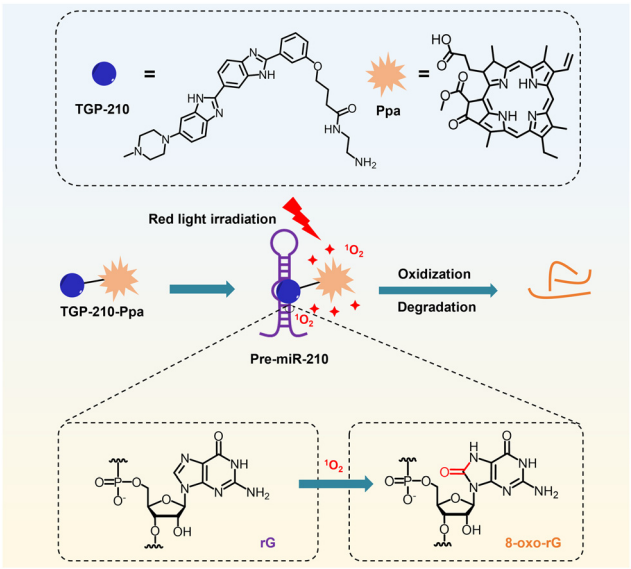


Scheme 1 Schematic illustration on the working mechanism of the ligand-directed red-light regulation of oncogenic microRNA.

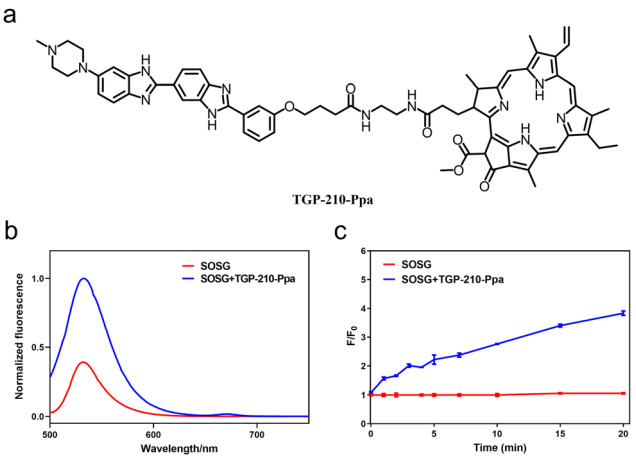


Fig. 1 (a) Chemical structure of **TGP-210-Ppa**. (b) Fluorescence spectra of **TGP-210-Ppa** after irradiation with 670 nm light (70 mW $cm^{-2}$) for 5 min. (c) The increase of SOSG fluorescence at 530 nm after incubation with **TGP-210-Ppa** and irradiation by 670 nm light (70 mW $cm^{-2}$) for 0–20 min. $\lambda_{ex}$ = 488 nm. Data are shown as mean ± SEM ($n$ = 3).

ultraviolet-visible (UV-Vis) spectroscopy of **TGP-210-Ppa** shows the characteristic absorption of **TGP-210** at ~350 nm and two characteristic absorption peaks of Ppa at ~400 nm and ~660 nm (Fig. S3, ESI†). The fluorescence spectrum shows that **TGP-210-Ppa** has similar fluorescence emission to that of Ppa (Fig. S4, ESI†). These results suggest that the conjugation of **TGP-210** to Ppa does not change the photophysical properties of the photo-sensitizer significantly.

We next examined whether **TGP-210-Ppa** was able to generate $^1O_2$ upon red-light irradiation and induce photo damage to its target pre-miR-210. Using the $^1O_2$ sensor green (SOSG) as the fluorescent indicator, we confirmed the capability of **TGP-210-Ppa** to generate $^1O_2$ in Phosphate Buffered Saline (PBS) buffer upon red light irradiation. As shown in Fig. 1b, irradiation of **TGP-210-Ppa** in PBS buffer containing SOSG using light of wavelength around 670 nm increased the fluorescence signal around 530 nm, which is characteristic of the fluorescence signal enhanced by $^1O_2$ on SOSG. Time dependence curve of the fluorescence enhancement *versus* irradiation time is shown in Fig. 1c. Subsequently, 9,10-anthracendipropionic acid (ADPA) was used as a capture probe to evaluate the efficiency of the $^1O_2$ generation. As shown in Fig. S5 (ESI†), the absorption intensity of ADPA at 378 nm gradually decreased as the irradiation time increased in the presence of the **TGP-210-Ppa** and MB, suggesting ADPA decomposition. According to the decay curves of the ADPA absorption, the $^1O_2$ quantum yield of the **TGP-210-Ppa** was about 0.327.[27] We then chose red light irradiation for 5 min as the standard condition to induce $^1O_2$-based oxidation.

Since nucleobases are known to be susceptible to $^1O_2$,[28] we evaluated the generation of oxidized nucleobases in pre-miR-210. Whether pre-miR-210 treated with **TGP-210-Ppa** upon red light irradiation results in the oxidation of nucleobases in pre-miR-210 was examined. We used LC-ESI-MS/MS to analyze the hydrolysis products of pre-miR-210 with or without **TGP-210-Ppa** under light irradiation (Fig. S6, ESI†). It is noteworthy that only 8-oxo-rG was detected as the oxidized nucleobase form in the hydrolyzed products of pre-miR-210 treated with **TGP-210-Ppa** and light irradiation. This is consistent with previous evidence that, among the four nucleobases in RNA, guanine is a major substrate of $^1O_2$.[29] Gel-shift assay revealed that excessive $^1O_2$ generated in the system by the presence of 200 equivalent of **TGP-210-Ppa** to pre-miR-210, together with 15 min light irradiation induced strand breakage (Fig. S7, ESI†), which is in agreement with previously reported results.[30,31] Overall, these results demonstrate that **TGP-210-Ppa** is able to cause oxidative damage to pre-miR-210 under photoirradiation.

The intracellular applications of **TGP-210-Ppa** were then explored. An MTT assay showed that **TGP-210-Ppa** had no obvious cytotoxicity in the dark at the concentration up to 25 μM (Fig. 2a). Confocal fluorescence imaging and flow cytometry showed that **TGP-210-Ppa** was able to be taken up

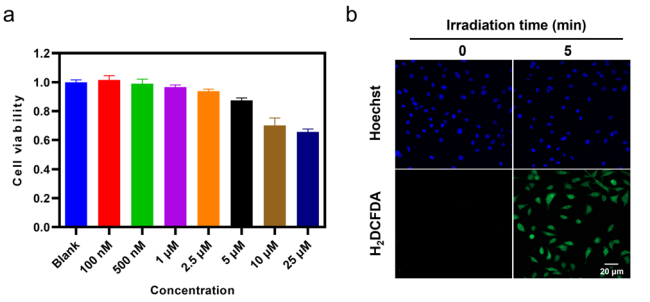


Fig. 2 (a) Relative viabilities of MDA-MB-231 cells incubated with different concentrations of **TGP-210-Ppa** for 48 h before light exposure. (b) Confocal microscopic images of MDA-MB-231 cells treated with **TGP-210-Ppa** for 4 h followed by exposure to 670 nm light for 5 min. Scale bar: 20 μm.

 

by cancer cell lines such as breast cancer MDA-MB-231 cells (Fig. S8, ESI†). Intracellular generation of $^1O_2$ by **TGP-210-Ppa** upon exposure to red light irradiation was monitored using the $^1O_2$-sensitive fluorescent probe 2′,7′-dichlorodihydrofluorescein diacetate ($H_2$DCFDA). As shown in Fig. 2b, the irradiation of MDA-MB-231 cells incubated with **TGP-210-Ppa** using light of 670 nm for 5 min significantly enhanced the fluorescence signal from the $^1O_2$ indicator inside the cells. We next investigated whether the *in-situ* generation of $^1O_2$ was able to regulate the intracellular pre-miR-210 since it was the target of **TGP-210-Ppa** for proximity-based regulation. Furthermore, to study the binding consequences of adding the Ppa moiety to **TGP-210**, binding affinities were measured by microscale thermophoresis (MST) to the targets with **TGP-210** or **TGP-210-Ppa**.[15,32] The results indicate that **TGP-210-Ppa** maintained selective binding to RNA with a $K_d$ of 392 nM to pre-miR-210, which is modestly weaker compared with **TGP-210** with a $K_d$ of 265 nM (Fig. S9, ESI†).

The protocol to evaluate the efficacy of the ligand-directed red-light regulation of intracellular pre-miR-210 is illustrated in Fig. 3a. Quantitative reverse transcription polymer chain reaction (qRT-PCR) results indicated the relative abundance of various RNAs in MDA-MB-231 cells treated with **TGP-210-Ppa** with or without red light irradiation. Cells treated by **TGP-210** or Ppa were used as a control to exclude the effect caused by the ligand or photo-sensitizer alone (Fig. 3b). Without exposure to light irradiation, both **TGP-210** and **TGP-210-Ppa** raised the intracellular level of pre-miR-210 dose-dependently, which could be attributed to the ligand-mediated blockade of pre-miR-210 processing due to the occupancy of enzymatic sites by **TGP-210-Ppa**.[33] Cells treated by Ppa alone did not show obvious changes in the intracellular pre-miR-210 level even after red light irradiation.

For cells treated by **TGP-210-Ppa** with a concentration as low as 10 nM, red light irradiation induced a significant decrease of intracellular pre-miR-210 level (Fig. 3c). Higher concentrations of **TGP-210-Ppa** elevated the pre-miR-210 level before light irradiation. However, after the cells pre-treated with **TGP-210-Ppa** were exposed to red light irradiation to trigger the formation of $^1O_2$, the ligand-directed modification or degradation of pre-miR-210 became predominant. These results suggest that the enhanced suppression of miR-210 by **TGP-210-Ppa** depends on both its chimeric effects. Also, **TGP-210-Ppa** further reduced the intracellular level of miR-210 in a dose-dependent manner under light irradiation, with similar effects observed for pre-miR-210 (Fig. S10, ESI†). Consequently, **TGP-210-Ppa** led to a more potent inhibition of miR-210 biogenesis after photo-irradiation. Moreover, non-target miRNAs, including miR-21, miR-24 and miR-192, were not modulated by **TGP-210-Ppa** even after light irradiation (Fig. 3d), confirming a ligand-directed selective inhibition of miR-210.

Finally, we investigated whether the ligand-directed photo-regulation of pre-miR-210 was able to further regulate relevant genes down-stream of miR-210. It has been well established that the overexpression of miR-210 promotes cancer cell growth by inhibiting the glycerol-3-phosphate dehydrogenase 1-like (GPD1L)-hypoxia inducible factor 1-alpha (HIF-1α) pathway (Fig. 4a).[34] Therefore we examined the potential of **TGP-210-Ppa** for photo-regulating the expression level of GPD1L and HIF-1α. The results shown in Fig. 4b and c confirmed our assumption that **TGP-210-Ppa** in MDA-MB-231 cells upon

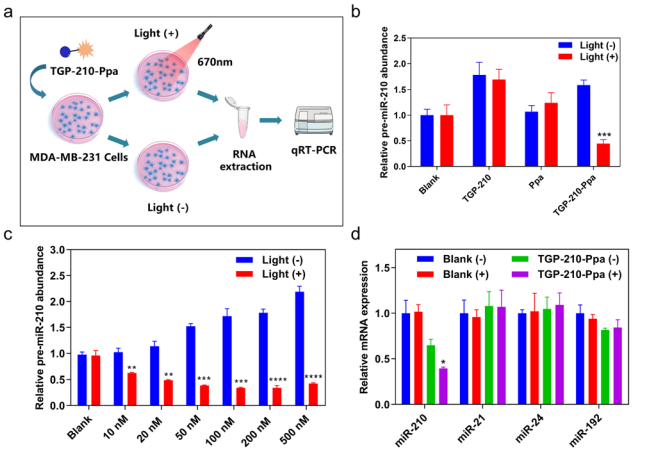


Fig. 3 (a) Schematic illustration of the protocol to evaluate the efficacy of the ligand-directed red-light regulation of intracellular pre-miR-210. (b) qRT-PCR analysis of pre-miR-210 in MDA-MB-231 cells pre-treated with **TGP-210** (500 nM), Ppa (500 nM) or **TGP-210-Ppa** (500 nM) before and after red light irradiation. Cells were incubated with different compounds for 4 hours, the red light applied was 670 nm light with intensity set at 70 mW cm$^{-2}$ and the irradiation time was 5 minutes. (c) Relative expression levels of pre-miR-210 in the different concentrations of **TGP-210-Ppa** treated groups with or without light. (d) Treatment of MDA-MB-231 cells with **TGP-210-Ppa** (500 nM) for 4 h and 670 nm irradiation for 5 min and 24 h later, qRT-PCR analysis of miR-210, miR-21, miR-24 and miR-192. Data are shown as mean ± SEM ($n$ = 3). *$P$ < 0.05, **$P$ < 0.01, ***$P$ < 0.001 and ****$P$ < 0.0001.

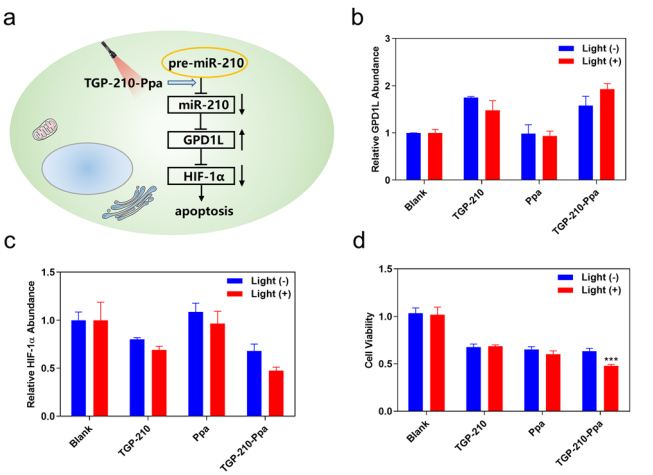


Fig. 4 (a) Schematic illustration of the miR-210-GPD1L-HIF1α regulatory pathway that might be photo-regulated in MDA-MB-231 cells treated by **TGP-210-Ppa**. (b) Quantitative analysis for GPD1L and (c) HIF-1α is measured by qRT-PCR with or without light. (d) Relative viabilities of MDA-MB-231 cells incubated with **TGP-210**, Ppa or **TGP-210-Ppa** for 4 h and 670 nm irradiation for 5 min at 24 h post incubation. Data are shown as mean ± SEM (n = 6). ***$P$ < 0.001.

photo-irradiation caused elevated expression of GPD1L and suppression of the HIF1α gene. MTT assay showed that **TGP-210-Ppa** with light irradiation elicited 52% cell apoptosis (Fig. 4d). Therefore, the ligand-directed photo-degradation of pre-miR-210 by **TGP-210-Ppa** could partially reverse the miR-210-involved signaling pathway to induce cancer apoptosis.

In summary, we reported a novel bifunctional chimera for photo-oxidation and degradation of target pre-miRNA that is related to cancer. **TGP-210-Ppa** that integrated the small-molecule ligand to the oncogenic pre-miR-210 with the photosensitizer Ppa was prepared, which demonstrated high efficacy for ligand-directed red-light degradation of intracellular pre-miR-210. **TGP-210-Ppa** could efficiently produce $^1O_2$ upon red-light irradiation, which induced the oxidization of rG into 8-oxo-rG in pre-miR-210 and further degradation of intracellular pre-miR-210. Using **TGP-210-Ppa** and red-light irradiation, we demonstrated the possibility of reversing oncogenic signalling pathways downstream of miR-210 to promote cancer cell apoptosis. As more small-molecule ligands are being reported to bind with specific RNA targets, this proof-of-concept work holds promise to develop various photo-regulatable bifunctional chimeras for spatial and temporal degradation of disease-related precursor microRNAs. Further efforts to address the limit of this system for *in vivo* applications due to the penetration ability of red light into deep tissue are now underway in our group.

This work was supported by the Natural Science Foundation of Jiangsu Province (BK20202004, BE2022835), the National Natural Science Foundation of China (22225703, 22137003, 22077063, 21877058, 21977043) and the Fundamental Research Funds for the Central Universities (020514380300).

## Conflicts of interest

There are no conflicts to declare.

## References

1 A. Abi, N. Farahani, G. Molavi and S. M. Gheibi Hayat, *Cancer Gene Ther.*, 2020, **27**, 280–293.
2 M. Garofalo, G. D. Leva and C. M. Croce, *Curr. Pharm. Des.*, 2014, **20**, 5328–5335.
3 M. Fan, M. Shan, X. Lan, X. Fang, D. Song, H. Luo and D. Wu, *Front. Pharmacol.*, 2022, **13**, 1033017.
4 S. T. Crooke, J. L. Witztum, C. F. Bennett and B. F. Baker, *Cell Metab.*, 2018, **27**, 714–739.
5 T. Felicetti and G. Manfroni, *Future Med. Chem.*, 2021, **13**, 1245–1248.
6 A. Murata, T. Fukuzumi, S. Umemoto and K. Nakatani, *Bioorg. Med. Chem. Lett.*, 2013, **23**, 252–255.
7 D. D. Vo, C. Staedel, L. Zehnacker, R. Benhida, F. Darfeuille and M. Duca, *ACS Chem. Biol.*, 2014, **9**, 711–721.
8 D. D. Vo, T. P. Tran, C. Staedel, R. Benhida, F. Darfeuille, A. Di Giorgio and M. Duca, *Chemistry*, 2016, **22**, 5350–5362.
9 N. Ankenbruck, R. Kumbhare, Y. Naro, M. Thomas, L. Gardner, C. Emanuelson and A. Deiters, *Bioorg. Med. Chem.*, 2019, **27**, 3735–3743.
10 J. L. Childs-Disney, X. Yang, Q. M. R. Gibaut, Y. Tong, R. T. Batey and M. D. Disney, *Nat. Rev. Drug Discovery*, 2022, **21**, 736–762.
11 P. Zhang, X. Liu, D. Abegg, T. Tanaka, Y. Tong, R. I. Benhamou, J. Baisden, G. Crynen, S. M. Meyer, M. D. Cameron, A. K. Chatterjee, A. Adibekian, J. L. Childs-Disney and M. D. Disney, *J. Am. Chem. Soc.*, 2021, **143**, 13044–13055.
12 S. M. Meyer, T. Tanaka, P. R. A. Zanon, J. T. Baisden, D. Abegg, X. Yang, Y. Akahori, Z. Alshakarchi, M. D. Cameron, A. Adibekian and M. D. Disney, *J. Am. Chem. Soc.*, 2022, **144**, 21096–21102.
13 Y. Tong, Q. M. R. Gibaut, W. Rouse, J. L. Childs-Disney, B. M. Suresh, D. Abegg, S. Choudhary, Y. Akahori, A. Adibekian, W. N. Moss and M. D. Disney, *J. Am. Chem. Soc.*, 2022, **144**, 11620–11625.
14 Y. Li and M. D. Disney, *ACS Chem. Biol.*, 2018, **13**, 3065–3071.
15 M. G. Costales, B. Suresh, K. Vishnu and M. D. Disney, *Cell Chem. Biol.*, 2019, **26**, 1180–1186.e1185.
16 X. Liu, H. S. Haniff, J. L. Childs-Disney, A. Shuster, H. Aikawa, A. Adibekian and M. D. Disney, *J. Am. Chem. Soc.*, 2020, **142**, 6970–6982.
17 P. Di Mascio, G. R. Martinez, S. Miyamoto, G. E. Ronsein, M. H. G. Medeiros and J. Cadet, *Chem. Rev.*, 2019, **119**, 2043–2086.
18 H. Sies, C. Berndt and D. P. Jones, *Annu. Rev. Biochem.*, 2017, **86**, 715–748.
19 W. K. Martins, N. F. Santos, C. S. Rocha, I. O. L. Bacellar, T. M. Tsubone, A. C. Viotto, A. Y. Matsukuma, A. B. P. Abrantes, P. Siani, L. G. Dias and M. S. Baptista, *Autophagy*, 2019, **15**, 259–279.
20 K. Jakubczyk, K. Dec, J. Kaldunska, D. Kawczuga, J. Kochman and K. Janda, *Pol. Merkuriusz Lek.*, 2020, **48**, 124–127.
21 J. Shi, D. Wang, Y. Ma, J. Liu, Y. Li, R. Reza, Z. Zhang, J. Liu and K. Zhang, *Small*, 2021, **17**, e2104722.
22 Y. Jiao, Y. Gao, J. Wang, H. An, Y. X. Li and X. Zhang, *Int. J. Pharm.*, 2022, **621**, 121805.
23 J. Wang, H. He, X. Xu, X. Wang, Y. Chen and L. Yin, *Biomaterials*, 2018, **171**, 72–82.
24 S. Nath and K. Moore, *Bio-Protoc.*, 2019, **9**, e3314.
25 K. Takemoto, *Nihon Yakurigaku Zasshi*, 2022, **157**, 238–243.
26 K. Miura, Y. Wen, M. Tsushima and H. Nakamura, *ACS Omega*, 2022, **7**, 34685–34692.
27 J. Ge, Q. Jia, W. Liu, M. Lan, B. Zhou, L. Guo, H. Zhou, H. Zhang, Y. Wang, Y. Gu, X. Meng and P. Wang, *Adv. Healthcare Mater.*, 2016, **5**, 665–675.
28 C. Fimognari, *Oxid. Med. Cell. Longevity*, 2015, **2015**, 358713.
29 A. M. Fleming, O. Alshykhly, J. Zhu, J. G. Muller and C. J. Burrows, *Chem. Res. Toxicol.*, 2015, **28**, 1292–1300.
30 P. I. Moreira, A. Nunomura, M. Nakamura, A. Takeda, J. C. Shenk, G. Aliev, M. A. Smith and G. Perry, *Free Radical Biol. Med.*, 2008, **44**, 1493–1505.
31 W. Martinet, G. R. de Meyer, A. G. Herman and M. M. Kockx, *Eur. J. Clin. Invest.*, 2004, **34**, 323–327.
32 M. H. Moon, T. A. Hilimire, A. M. Sanders and J. S. Schneekloth, Jr., *Biochemistry*, 2018, **57**, 4638–4643.
33 M. G. Costales, C. L. Haga, S. P. Velagapudi, J. L. Childs-Disney, D. G. Phinney and M. D. Disney, *J. Am. Chem. Soc.*, 2017, **139**, 3446–3455.
34 S. Grosso, J. Doyen, S. K. Parks, T. Bertero, A. Paye, B. Cardinaud, P. Gounon, S. Lacas-Gervais, A. Noel, J. Pouyssegur, P. Barbry, N. M. Mazure and B. Mari, *Cell Death Dis.*, 2013, **4**, e544.

 